J. Fluid Mech. (1996), vol. 326, pp. 321–341
Copyright © 1996 Cambridge University Press

On the formation of longitudinal vortices in a turbulent boundary layer over wavy terrain

By W. R. C. PHILLIPS[1], Z. WU[2] AND J. L. LUMLEY[3]

[1] Department of Theoretical and Applied Mechanics, University of Illinois at Urbana-Champaign, Urbana, IL 61801-2935, USA

[2] Department of Mechanical and Aeronautical Engineering, Clarkson University, Potsdam, NY 13699-5725, USA

[3] Sibley School of Mechanical and Aerospace Engineering, Upson and Grummun Halls, Cornell University, Ithaca, NY 14853-7501, USA

(Received 15 January 1996, and in revised form 28 May 1996)

Parallel inviscid $O(1)$ shear interacting with $O(\epsilon)$ spanwise-independent neutral rotational Rayleigh waves are used to model turbulent boundary layer flow over small-amplitude rigid wavy terrain. Of specific interest is the instability of the flow to spanwise-periodic initially exponentially growing longitudinal vortex modes via the Craik–Leibovich CL2-$O(1)$ instability mechanism and whether it is this instability mechanism that gives rise to longitudinal vortices evident in the recent experiments of Gong *et al.* (1996). In modelling the flow, wave and turbulence length scales are assumed sufficiently disparate to cause minimal interaction. This allows the primary mean velocity profile to be specified. Two profiles were chosen: a power law and the logarithmic law of the wall. Important in wave–mean interactions of this class are the effect of wave-induced fluctuations upon the mean state and the influence of the developing mean flow on the fluctuating part of the motion. The former is described by a generalized Lagrangian-mean formulation; the latter by a modified Rayleigh equation. Together they comprise an eigenvalue problem for the growth rate appropriate to the initial stages of the instability. Both primary mean flows are unstable to longitudinal vortex form in the presence of Rayleigh waves whose amplitudes diminish with altitude. Moreover the interaction is most unstable for streamwise wavenumbers $\alpha = O(1)$, the growth rate increasing with increased spanwise wavenumber. In comparing the results with experiment, it is first shown that spanwise-independent waves excited in Gong *et al.*'s experiment depict velocity fluctuations whose amplitudes diminish with altitude in accord with those for appropriate Rayleigh waves. Concordantly, the longitudinal vortices depict transverse velocity components that are weaker by a factor of ϵ than the axial perturbation and are observed to grow at a rate consistent with exponential growth. All are key features of CL2-$O(1)$, although the observed growth rate is not in accord with the maximal suggested by inviscid instability theory. Rather it appears that the spanwise wavenumber takes a value at which energy is extracted from the mean motion in an optimal volume-averaged sense while minimizing energy loss to both viscous dissipation and small-scale turbulence. It is concluded that the CL2-$O(1)$ instability mechanism is physically realizable and that the data of Gong *et al.* represent the first documented observations thereof.

1. Introduction

Longitudinal vorticies have long been observed beneath (Langmuir 1938) and above (LeMone 1973) the wind-driven surface of open bodies of water. Each affect the water surface: for example Langmuir circulations concentrate flotsom or other organic materials into streaks or bands, while circulations in the atmosphere affect the short-scale sea roughness which synthetic aperture radar likewise depicts as streaks or bands (Alpers & Brümmer 1994), as does cold air advecting over warm water but visually (Stull 1988). In each instance the streaks indicate that the vortices are more or less aligned with the wind and of course the fact that they affect the surface suggests a close proximity to it. But while the spanwise scale of Langmuir cells is typically a few to several hundred metres (Leibovich 1983), atmospheric cells are of the order of kilometres. The presence of such cells is thought to greatly influence heat, mass and momentum transport properties both within and between the lower atmosphere and upper ocean, features that raise the question, do atmospheric cells also occur over land? The answer is probably yes (particularly above wavy terrain, see Hunt, Lalas & Asimakopoulos 1984), although the absence of evidence, *vis a vis* clearly defined footprints, has left the concept moot. Such vortices have, however, been observed in the experiments of Gong & Taylor (see Hunt *et al.* 1991) and by Gong, Taylor & Dörnbrack (1996), but unclear here is the mechanism by which the vortices form.

Gong *et al.* conducted a wind tunnel study of neutrally stratified zero pressure gradient turbulent boundary layer flow over two (aerodynamically) rough rigid undulating surfaces that comprise 16 small-amplitude spanwise-independent sinusoidal waves. Steady circulations with vorticity aligned with the mean motion were observed by the fourth wave, at which point the flow was approximately streamwise periodic and the boundary layer about one undulation wavelength thick. Interestingly, circulations were observed only above the smoother waves where the flow remained attached, whereas with the rougher waves it separated in the troughs.

Longitudinal vortices in the presence of mean shear and small-amplitude (spanwise independent) two-dimensional waves bring to mind the Craik–Leibovich type-2 or CL2 instability mechanism, which Craik (1977) and Leibovich (1977) put forward to explain the presence of Langmuir circulations in the upper ocean. In such circumstances the wind-induced shear is weak, typically $O(\epsilon^2)$ in the presence of $O(\epsilon)$ surface gravity waves, where ϵ is a small parameter characteristic of the wave slope. The ensuing interaction is unstable and gives rise to longitudinal vortices that grow exponentially fast whenever the gradients of both the mean velocity and the Stokes drift are in the same sense. We denote this form of the instability CL2-$O(\epsilon^2)$.

But in Gong *et al's* experiment, and in the atmosphere, the mean shear is significantly stronger than $O(\epsilon^2)$. Craik (1982*b*) has shown that CL2 continues to operate in $O(1)$ shear, although now another measure of nonlinear rectification (of the waves both with themselves and the shear), the pseudomomentum, replaces Stokes drift as the catalyst for instability. Furthermore wave distortion, which is negligible in CL2-$O(\epsilon^2)$, here plays an important role by acting to diminish the instability (Phillips & Wu 1994). And finally, instability to longitudinal vortex form occurs whenever, from the reference frame of the waves, and in the direction of increasing mean flow, the relative increase in mean flow exceeds the relative increase in wave amplitude (Craik 1982*b*; Phillips & Shen 1996). To date only two cases of CL2-$O(1)$ have been treated in detail: uniform shear between rigid wavy walls and exponentially decaying shear beneath surface gravity waves (Phillips & Wu). But the CL2-$O(1)$ instability is

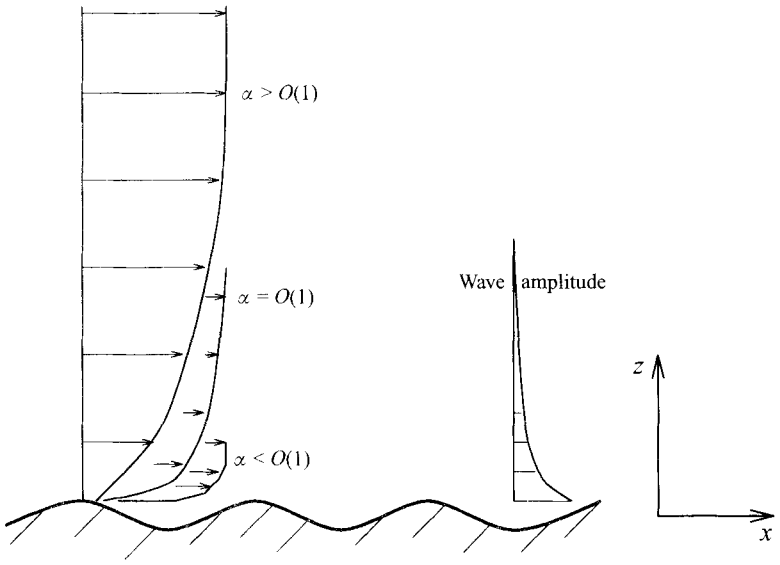

FIGURE 1. Sketch of flow over wavy terrain showing the non-dimensional streamwise wavenumber $\alpha = 2\pi\delta/\lambda$ as it relates to the characteristic thickness of the boundary layer δ and terrain wavelength λ. Shown also is the amplitude of the wave-induced flow perturbation.

ubiquitous over a wide range of physically interesting wave–mean flow interactions (Phillips & Shen): in particular these authors show that boundary layer profiles, when viewed from the reference frame of the waves, in this instance the wavy wall, are unstable (to longitudinal vortex form) only in the presence of what they term type-2 Rayleigh waves, i.e. waves whose amplitudes diminish with distance from the wall. To wit, just the class of waves we should expect when a boundary layer is perturbed by wavy terrain and just the class observed by Gong *et al.*. There is thus a *prima facie* case that the circulations observed by Gong *et al.* are excited by the CL2-$O(1)$ instability, which if true would represent the first documented observation of CL2-$O(1)$. Our intent here, therefore, is to provide further details of CL2-$O(1)$ in the configuration studied by Gong *et al.*, with a view to ascertain whether the instability they observe is or is not CL2-$O(1)$.

Specifically we model the mean turbulent boundary layer by an inviscid parallel $O(1)$ shear flow and consider the instability (to longitudinal vortex form) of that flow to $O(\epsilon)$ two-dimensional spanwise-independent waves, assumed generated by a rigid wavy wall as sketched in figure 1. We assume from the outset that the wave and turbulence length scales are sufficiently disparate to cause minimal interaction, the turbulence scales being smaller. In consequence we need concern ourselves only with the mean (i.e. streamwise averaged) velocity profile. We further assume that although viscosity acts to give rise to the mean velocity profile, it plays no further significant role. The boundary layer thus perceives undulations in the rigid wall as slippery wave generators that give rise to waves which satisfy the Rayleigh equation. That is, the waves are Rayleigh waves defined by the mean shear flow and amplitude of the wavy wall. We approximate the mean velocity profile first by a power law (§§4.1–4.3) (because it has clear analytical advantages in determining admissible Rayleigh waves) and second by the logarithmic law of the wall (§4.4) which, while more representative of observation, necessitates the numerical solution of Rayleigh's equation (§3.1). The ensuing inviscid nonlinear wave–mean interaction is described in

part by the generalized Lagrangian-mean equations of Andrews & McIntyre (1978), which contract, for rectilinear flows, to an eigenvalue problem for the growth rate of spanwise-periodic longitudinal vortices (Craik 1982*b*). The Rayleigh–Craik equation, which accounts for wave distortion due to mean flow anomalies, completes the specification (§2). The results are reported in §4, compared with the experimental data of Gong *et al.* in §5, and are discussed in §6.

2. Background

2.1. *The generalized Lagrangian-mean equations*

The ubiquity of wave activity in geophysics has long necessitated the need for a rational way to separate 'wave' from 'mean' flow and to define wave–mean interactions, and the path to this end culminated with the generalized Lagrangian-mean equations of Andrews & McIntyre (1978). These equations describe the back effect of oscillatory disturbances upon the mean state and are exact provided the mapping between the true Lagrangian and reference generalized Lagrangian-mean (GLM) remains invertible; GLM is thus valid for rotational waves of any amplitude but is of doubtful validity in the vicinity of critical layers, unless the critical layer occurs at a rigid boundary. The Lagrangian-mean velocity so described, however, is not the 'mean following a single fluid particle'; rather it is the velocity field describing trajectories about which the fluctuating particle motions have zero mean, when *any* averaging process is applied. Here the choice is a streamwise average at fixed z. To express ideas like 'steady mean flow', an Eulerian description of the GLM, with position $\boldsymbol{x}$ and time t as independent variables, is employed, so that the GLM formulation is really a hybrid Eulerian–Lagrangian description of wave–mean flow interactions. Then provided the abovementioned mapping is invertible, there is, for any given Eulerian velocity $\boldsymbol{u}(\boldsymbol{x}, t)$, a unique 'related velocity field' $\bar{\boldsymbol{u}}^L$, which is the Lagrangian-mean velocity such that $\bar{\boldsymbol{u}}^L$ is related to the Eulerian-mean velocity by the generalized Stokes drift $\bar{\boldsymbol{d}}$, as $\bar{\boldsymbol{u}}^L = \bar{\boldsymbol{u}} + \bar{\boldsymbol{d}}$.

Andrews & McIntyre derive equations for the GLM motion from the compressible Navier–Stokes equations, and for homentropic flows of constant density in a non-rotating reference frame, the GLM momentum equation is, in the absence of dissipation and pressure gradients,

$$\bar{\mathrm{D}}^L(\bar{u}_i^L - p_i) + \bar{u}_{k,i}^L(\bar{u}_k^L - p_k) = 0, \tag{2.1}$$

where repeated indices imply summation, commas denote differentiation and $(x_1, x_2, x_3) \equiv (x, y, z)$. The operator $\bar{\mathrm{D}}^L$ is defined as $\bar{\mathrm{D}}^L = \partial_{,t} + \bar{u}_j^L \partial_{,x_j}$; and the vector wave property p_i, the pseudomomentum per unit mass, is a measure of the nonlinear rectification of oscillatory disturbances both with themselves and the mean shear flow. Further details are given elsewhere (Andrews & McIntyre 1978; Craik 1985).

2.2. *O(1) shear and O(ϵ) waves*

Consider the interaction between an $O(1)$ primary shear flow and two-dimensional straight-crested periodic waves. Then with space coordinates (x, y, z), and in the reference frame of the waves which is here that of the terrain, our primary shear flow in $[z_1, z_2]$ is $\bar{u}(z)$. We shall assume that viscosity is important only so far as giving rise to the mean velocity profile, and employ length and velocity scales that lead to the scaling $\bar{u}(1) = 1$. The waves are (initially) spanwise-independent and of constant amplitude with slope characterized by the small parameter ϵ; so provided critical

layers ($\bar{u} = 0$) occur only at boundaries and not in the interior of the primary flow, then the temporal growth or decay rate of the waves is zero and they induce an $O(\epsilon^2)$ pseudomomentum field $\boldsymbol{p} = [p_1, 0, 0]$.

Envisage now small spanwise-periodic perturbations with Eulerian velocity components of the form

$$(\tilde{u}, \tilde{v}, \tilde{w}) = \Delta \mathrm{Re}\{e^{\sigma t} e^{ily} [\hat{u}(z), -\epsilon^n i\hat{v}(z), \epsilon^n \hat{w}(z)]\} \tag{2.2}$$

which, provided the amplitude field of the waves is steady, satisfy continuity correct to $O(\epsilon^2)$ as

$$l\hat{v} + \hat{w}_{,z} = 0. \tag{2.3}$$

Here Δ measures the strength of this motion relative to the primary shear flow and is assumed sufficiently small that linearization with respect to it yields a good approximation to the equations governing the spanwise-periodic disturbance; σ is the growth rate of the spanwise perturbation. In view of our rigid wavy wall at say $z = z_1$ and a wave of smaller or zero amplitude at say $z = z_2$ (which for specificity we consider as rigid), we impose zero wave and velocity distortion at both, i.e.

$$\hat{w} = \hat{\phi} = 0 \quad \text{at} \quad z = z_1, z_2 \tag{2.4}$$

where $\hat{\phi}$ is defined below. Of course for instability, (2.1) and (2.3) must admit non-trivial solutions for such boundary conditions and that requires $n = 1$ (Craik 1982*b*). As is evident from (2.2), velocity perturbations in the y- and z-directions are therefore weaker by a factor of ϵ than the x velocity perturbation; concordantly $\sigma_0 = 0$ in the expansion for σ, leaving $\sigma = \epsilon\sigma_1 + O(\epsilon^2)$. Thus (2.1) and (2.3) reduce to

$$\sigma_1 \hat{u} = -\hat{w}\bar{u}_{,z}, \tag{2.5}$$

$$\hat{w}_{,zz} + l^2 \left[\frac{P_{1,z}\bar{u}_{,z}}{\sigma_1^2} - 1 \right] \hat{w} = -\frac{l^2 \bar{u}_{,z}}{\sigma_1} \hat{p}_1. \tag{2.6}$$

Observe that two components of the pseudomomentum

$$p_1 = \epsilon^2 P_1(z) + \epsilon^2 \Delta \mathrm{Re}\{e^{\sigma t} e^{ily} \hat{p}_1(z)\} + O(\epsilon^4, \epsilon^3\Delta, \epsilon^2\Delta^2), \tag{2.7}$$

play a role. The first, due to the x-periodic perturbation field $\tilde{u}_i = \epsilon \mathrm{Re}[\phi_{,z}, 0, -i\alpha\phi] + O(\epsilon\Delta, \epsilon^2, \epsilon\Delta^2)$, is (Craik 1982*a*)

$$P_1 = -\frac{\bar{u}}{2} \left\{ \left| \left(\frac{\phi}{\bar{u}} \right)_{,z} \right|^2 + \alpha^2 \left| \frac{\phi}{\bar{u}} \right|^2 \right\}, \tag{2.8}$$

where $\phi(z)$ and α (see also §4) denote the eigenfunction and non-dimensional wavenumber of the primary (i.e. $O(\epsilon)$ component of the) wave field which together satisfy Rayleigh's equation,

$$\bar{u}(\phi_{,zz} - \alpha^2\phi) - \bar{u}_{,zz}\phi = 0. \tag{2.9}$$

The second component, $\mathrm{Re}\{e^{ily}\hat{p}_1\}$, is the spanwise-periodic perturbation of pseudomomentum due to distortion of the primary wave field by the emerging secondary Eulerian velocity field.

Unfortunately the GLM formulation provides no direct means of evaluating $\hat{p}_1$ so a separate examination of the wave field is necessary. On doing so, Craik (1982*b*) found that

$$\hat{p}_1 = \mathscr{A}(z)\hat{u}(z) + \mathscr{B}(z)\hat{u}_{,z}(z) + \mathrm{Re}\left\{ \mathscr{C}(z)\hat{\phi}(z) + \mathscr{D}(z)\hat{\phi}_{,z}(z) \right\}, \tag{2.10}$$

where $\mathscr{A}$, $\mathscr{B}$, $\mathscr{C}$ and $\mathscr{D}$ are functions which are independent of σ, and that $\hat{\phi}(z)$, which relates to the $O(\epsilon A)$ spanwise-periodic wave field modification, satisfies the Rayleigh–Craik equation

$$\bar{u}[\hat{\phi}_{,zz} - (\alpha^2 + l^2)\hat{\phi}] - \bar{u}_{,zz}\hat{\phi} = -\hat{u}[\phi_{,zz} - (\alpha^2 + l^2)\phi] + \hat{u}_{,zz}\phi, \tag{2.11}$$

in which l is the spanwise wavenumber.

Thus given the primary shear flow $\bar{u}$ and, from (2.9), the primary wave field eigenfuction ϕ along with appropriate boundary conditions, the eigenvalue problem for σ_1 is completely specified by the coupled system (2.5), (2.6) and (2.11), together with (2.8) and (2.10).

3. Numerical procedure

3.1. *Numerical solution of the Rayleigh equation*

Rayleigh's equation (2.9) is soluble analytically for mean velocity profiles that obey a power law (Phillips & Shen 1996; see also §4) but that is not the case for logarithmic or most other profiles. To proceed therefore we require a numerical scheme commensurate with that for solving our eigenvalue problem (§3.2), specifically one using Galerkin techniques. In outlining the technique, we shall restrict attention to phase velocities that are real, although of course the technique is readily extendible to complex phase velocities. We shall also restrict attention to waves whose amplitudes diminish as $\alpha z \to \infty$, i.e. Rayleigh waves of the second kind (see §4.1); appropriate boundary conditions to (2.9) on the semi-infinite domain $z \in [z_1, \infty]$ are thus

$$\phi(z_1) = \phi_1, \quad \phi(\infty) = 0, \tag{3.1}$$

where z_1 and ϕ_1 are arbitrary constants.

For computational reasons, however, the semi-infinite domain is less desirable than a finite domain and so we employ the transform $\xi = \mathrm{e}^{-z}$. Then on writing $F(\xi) = \bar{u}_{,zz}/\bar{u}$, (2.9) becomes

$$\xi^2\phi_{,\xi\xi} + \xi\phi_{,\xi} - (\alpha^2 + F(\xi))\phi = 0 \tag{3.2}$$

with the boundary conditions

$$\phi(0) = 0, \quad \phi(\xi_1) = \phi_1, \tag{3.3}$$

where $\xi_1 = \mathrm{e}^{-z_1}$.

Our intent is to solve (3.2) by Galerkin techniques and thus suppose $\phi(\xi)$ can be expressed as

$$\phi(\xi) = \psi(\xi) + \sum_{i=1}^{N} a_i f^i(\xi), \tag{3.4}$$

where $\psi(\xi)$ is an arbitrary function which satisfies the boundary conditions (3.3) and $f^i(\xi)$ are basis functions (in this instance Chebyshev polynomials) that satisfy homogeneous boundary conditions

$$f^i(\xi_1) = f^i(0) = 0. \tag{3.5}$$

Finally, a_i are coefficients of the expansion and N is an integer large enough to make the expansion a close approximation to ϕ.

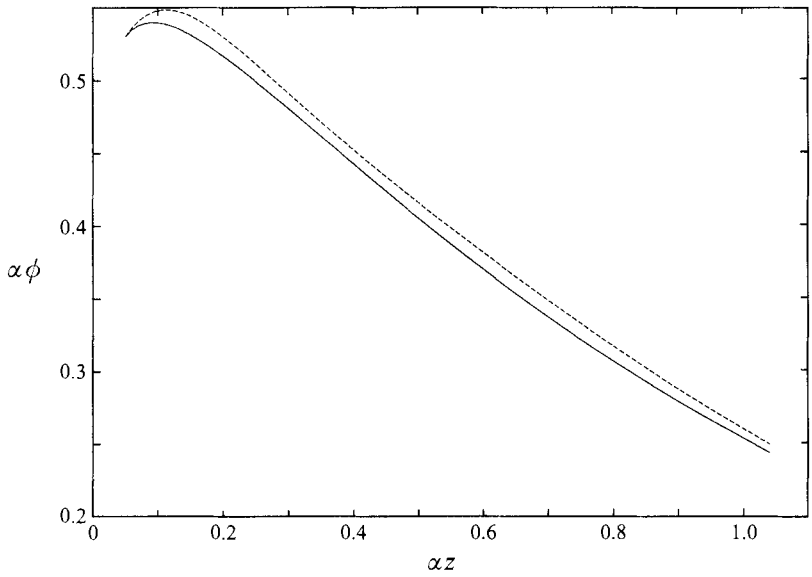

FIGURE 2. Solution of the Rayleigh equation for wave amplitude, $\alpha\phi$, for type-2 waves, for the power-law (solid line) and logarithmic law (dashed line) mean velocity profiles; for $\alpha = 1$.

Substitution of (3.4) into (3.2) then yields the residual

$$R(\xi) = \xi^2\psi_{,\xi\xi} + \xi\psi_{,\xi} - (\alpha^2 + F(\xi))\psi + \sum_{i=1}^{N} a_i[\xi^2 f^i_{,\xi\xi} + \xi f^i_{,\xi} - (\alpha^2 + F(\xi))f^i], \quad (3.6)$$

which is required to satisfy

$$\langle R(\xi),\ f^j(\xi)\rangle = 0; \quad j = 1, 2, \cdots, N,$$

where the inner product is

$$\langle g,\ h\rangle = \int_a^b g(s)h(s)\mathrm{d}s$$

for continuous functions $g(s)$ and $h(s)$ defined in $[a, b]$.

This results in N linear algebraic equations for a_i which can be written in the form

$$\mathscr{E}_{ij}a_j = \mathscr{F}_i, \quad (3.7)$$

where coefficients of the $N \times N$ matrix $\mathscr{E}_{ij}$ and $N \times 1$ matrix $\mathscr{F}_i$ are defined as

$$\mathscr{E}_{ij} = \langle f^i(\xi),\ \xi^2 f^j_{,\xi\xi} + \xi f^j_{,\xi} - (\alpha^2 + F(\xi))f^j(\xi)\rangle,$$
$$\mathscr{F}_i = -\langle f^i(\xi),\ \xi^2\psi_{,\xi\xi} + \xi\psi_{,\xi} - (\alpha^2 + F(\xi))\psi(\xi)\rangle.$$

Then, with the coefficients a_j at hand, we can recover $\phi(\xi)$ and ultimately $\phi(z)$.

To test the procedure calculations were made using power-law profiles for $\bar{u}$; with $N = 20$ the technique realized $\phi(z)$ profiles for each q (see §4.2) closely in accord with the analytical solution (4.2). Finally, we see in figure 2 that distributions in wave amplitude for a logarithmic profile (4.6) are not greatly different from those for a one-seventh power-law, boundary conditions (i.e. wave amplitude) being identical at an appropriate elevation z_1 in each case.

3.2. *Solution of the eigenvalue problem*

Galerkin techniques were also used to solve the eigenvalue problem (2.5), (2.6) and (2.11) for the eigenvalue σ_1, which because (2.6) and (2.11) are real, may be real, imaginary or a complex conjugate pair. Complete details are given in Phillips & Wu (1994). Briefly, we suppose $\hat{u}(z)$ and $\hat{\phi}(z)$ can be expanded in linearly independent complete sets of basis functions $u_i(z)$ and $\phi_i(z)$ as

$$\hat{u}(z) = \sum_{i=1}^{M} b_i u_i(z), \quad \hat{\phi}(z) = \sum_{i=1}^{M} b_{M+i}\phi_i(z), \tag{3.8}$$

where b_i and b_{M+i} are the expansion coefficients of $\hat{u}(z)$ and $\hat{\phi}(z)$ respectively, and M is integer. The basis functions were chosen to satisfy the boundary conditions (2.4), which suggest we set $u_i(z) = \phi_i(z)$.

Substitution of (3.8) into (2.6) and (2.11) then leads to the residual functions $R_u(z)$ and $R_\phi(z)$ which must satisfy the inner products

$$\langle R_u(z),\ u_j(z)\rangle = 0; \quad \langle R_\phi(z),\ \phi_j(z)\rangle = 0.$$

A $2 \times M$-order linear eigenvalue problem for λ^2, where $\lambda = l/\sigma_1$, results as

$$\mathscr{L} = \lambda^2 \mathscr{M}, \tag{3.9}$$

where $\mathscr{L}$ and $\mathscr{M}$ are $2M \times 2M$-order matrices with components that are $M \times M$-order sub-matrices; specifically, the components are functions of α and l, but not σ_1.

Of interest is the largest real eigenvalue σ_1, or if no real values occur the complex value with the largest real part, for each pair (α, l) and the eigenfunctions $\hat{u}$ and $\hat{\phi}$. Chebyshev polynomials were used as basis functions and the accuracy provided by the $M = 20$ expansion was considered adequate for our purposes. All computations were performed on a DECstation 5000/200 using double-precision arithmetic with IMSL routines to solve the eigenvalue problem (3.9).

4. Boundary layer flow over wavy terrain

Boundary layer flow over wavy terrain is characterized by two length scales: the wavelength of the undulations λ and a measure of the thickness δ of the boundary layer that is formed over them; both are captured in the non-dimensional streamwise wavenumber $\alpha = 2\pi\delta/\lambda$. Thus, since type-2 Rayleigh waves are most influential over $\alpha z = O(1)$ (see figure 2), three categories of boundary-layer/terrain interaction are evident: in the first the extent of the boundary layer well exceeds that of the wave field and so $\alpha > O(1)$; in the second the boundary layer and wave field are of similar extent so $\alpha = O(1)$, and in the third the wave field extends far beyond the boundary layer, yielding $\alpha < O(1)$. Each is sketched in figure 1. Accordingly the spanwise spacing of longitudinal cells which form is L, so that $l = 2\pi\delta/L$, and because it is doubtful whether cells excited by CL2-$O(1)$ extend beyond either the boundary layer or the wave field, it follows that $l \geqslant \sup\{\alpha\pi/6\gamma, \pi/\gamma\}$, where γ is the aspect ratio, i.e. width/height of the cells. Our intent then is to consider a range of α that captures each of the three categories with an appropriate range of l throughout.

4.1. *Power-law mean velocity profile*

As our first example we consider the shear flow $\bar{u} = z^q$ in $[z_1, z_2]$, with $z > 0$ and q a real positive number, upon which is superposed a two-dimensional neutral-wavelike-disturbance $\alpha\phi$ which satisfies the Rayleigh equation (2.9). Since the wall region and

thus $z = 0$ are not of interest, our calculation domain is chosen as $[z_1, 1 + z_1]$, where z_1 is slightly larger than zero. In the course of our study various values of $0 < z_1 \ll 1$ were employed. It transpired that z_1 affected the magnitude but had little influence on the generic form of $\sigma_1(\alpha, l)$, so z_1 was chosen such that $\sigma_1(1, \infty)$, which remained $O(1)$ for all admissible z, was approximately unity, which is the case when $z_1 = 0.05$.

4.2. *Rayleigh waves*

Admissible Rayleigh waves for the mean velocity profile $\bar{u} = z^q$ follow by substitution of $\alpha\phi = \zeta^{1/2}\Phi$ and $\zeta = \alpha z$ into (2.9) to yield the modified Bessel equation

$$\Phi_{,\zeta\zeta} + \frac{1}{\zeta}\Phi_{,\zeta} - \left(1 + \frac{(q - \frac{1}{2})^2}{\zeta^2}\right)\Phi = 0$$

which has the general solution,

$$\Phi = A_1 I_{\pm(q-1/2)}(\zeta) + A_2 K_{q-1/2}(\zeta). \tag{4.1}$$

Here $I_{\pm(q-1/2)}(\zeta)$ and $K_{q-1/2}(\zeta)$ are the modified Bessel functions (Abramowitz & Stegun 1965) and A_1, A_2 arbitrary constants. Observe that as $\zeta \to 0$, $I_{\pm(q-1/2)}$ is bounded while $K_{q-1/2}$ depicts a logarithmic singularity; conversely as $\zeta \to \infty$, $K_{q-1/2}$ is bounded while $I_{\pm(q-1/2)}$ is unbounded. Phillips & Shen (1996) have shown that boundary layer profiles of the class $\bar{u} = \pm|z|^q$ with $0 < q \ll 1$ are unstable to longitudinal vortex form only in the presence of waves for which the wave amplitude $\alpha\phi$ diminishes as $\alpha z \to \infty$, i.e. Rayleigh waves of the second kind. We thus set $A_1 = 0$ and $A_2 = 1$, so

$$\alpha\phi = (\alpha z)^{1/2} K_{q-1/2}(\alpha z) \quad (0 < \alpha z < \infty). \tag{4.2}$$

Straightforward analysis then yields the pseudomomentum

$$P_1^0(z) = -\frac{\alpha z^{1-q}}{2}[K_{q+1/2}^2 + K_{q-1/2}^2]$$

from which we find (see (2.6)) that

$$\bar{u}_{,z} P_{1,z}^0(z) = q\alpha^2 \left\{ (K_{q+1/2}K_{q+3/2} + K_{q-1/2}K_{q+1/2}) - \frac{1}{2\alpha z}\left((q+2)K_{q+1/2}^2 + qK_{q-1/2}^2\right) \right\}, \tag{4.3}$$

K being a function of αz in all cases.

If we further assume that the mean velocity profile is closely approximated by setting $q = \frac{1}{7}$, then the amplitude distribution $\alpha\phi$ and the gradient product $\bar{u}_{,z} P_{1,z}^0(z)$ are unique.

4.3. *Results*

Of particular interest is the growth rate σ_1 and its variation with α and l. We begin by determining σ_1 in a range where the most analytical progress can be made, namely the limit $l^2 \gg \alpha^2$ for $\alpha = O(1)$ (see Craik 1982*b*; Phillips & Shen 1996). This limit is realizable in nature although vortices have not as yet been observed at the larger spanwise wavenumbers (see §6), in particular as $l^2 \to \infty$, where, as we shall see, the growth rate is largest. Nevertheless, the asymptotic limit $l^2 \to \infty$ provides a useful check for our numerics.

For reference purposes we first exclude wave distortion, i.e. set $\hat{p}_1 = 0$. In such circumstances two linearly independent solutions to (2.6), λ_A and λ_B, may be constructed via the WKBJ approximation. Then λ_A, $\lambda_B = -\frac{1}{2}\sigma_1^{-2}\bar{u}_{,z} P_{1,z}^0[1 \pm 1]$ and it

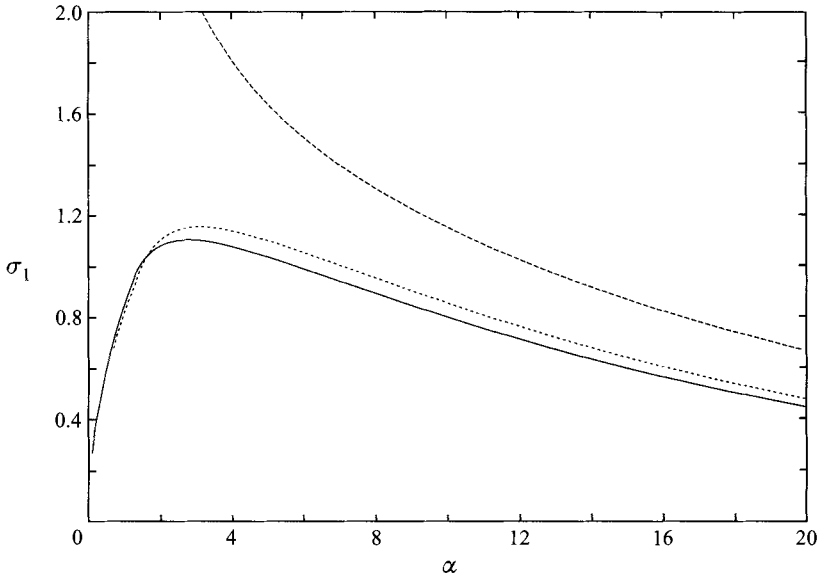

FIGURE 3. Variation of the growth rate σ_1 with streamwise wavenumber α in the limit $l^2 \to \infty$: the analytical solution (4.4) (long dashes) in the absence of wave distortion; and numerical solution for a power-law (solid line) and logarithmic (short dashes) mean velocity profile.

follows (see Craik 1982*b*) that non-trivial solutions exist only if $\sigma_1^{-2}\bar{u}_{,z}P^0_{1,z}$ is greater than unity. Thus the largest upper bound for σ_1 must occur when $\bar{u}_{,z}P^0_{1,z}$ is a maximum (in this instance at $z = z_1$) and $\sigma_1^{-2}\bar{u}_{,z}P^0_{1,z}$ is minimum, i.e. approaching unity from above, so that

$$\sigma_1^2 \sim \lim_{z \to z_1} \bar{u}_{,z}P^0_{1,z} \quad (\alpha \neq 0, \quad l^2 \to \infty), \tag{4.4}$$

and our numerics concur. Unfortunately, an analytical solution for the case with wave distortion (i.e. with $\hat{p}_1 \neq 0$) is not forthcoming so we must rely solely on numerics. The ensuing growth rates for both the distortion and non-distortion (4.4) case are depicted in figure 3. Observe that in accord with the cases studied by Phillips & Wu (1994), wave distortion acts to diminish the growth rate; however while they observed diminution only for wavenumbers $\alpha \leqslant O(1)$, diminution is here evident to much larger wavenumbers. Note also that σ_1 is maximum when $\alpha = O(1)$. This result concurs with Phillips & Wu's finding for an exponentially decaying velocity profile beneath surface gravity waves but is in marked contrast to their result for uniform shear between rigid wavy walls, where σ_1 is a maximum in the long-wave limit $\alpha \to 0$. The contrast is apparently due to the type of wave field, which is irrotational in the presence of uniform shear but rotational in the presence of non-uniform shear.

Looking now to the double long-wave limit $\alpha \to 0$, $l \to 0$, we observe two very different regimes: in the first, denoted I, the most unstable growth rate σ_1 is real and follows the pattern depicted in figure 4. But in the second, denoted II, σ_1 appears only as complex conjugate pairs. Similar behaviour was observed and investigated in detail by Phillips & Wu. Specifically in region II, the flow remains unstable to longitudinal vortex form but the vortices are subject to a standing oscillation, i.e they stand in space and alternate in sign; there is also the possibility of vortices propagating spanwise at equal and opposite speed. Moreover, in view of the bound

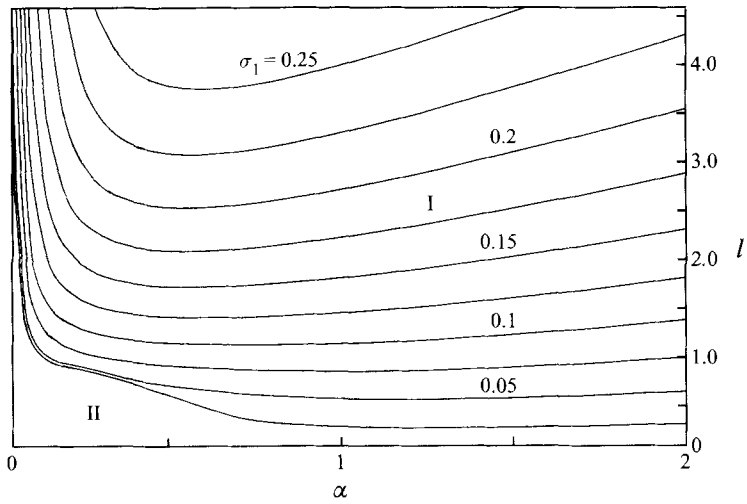

FIGURE 4. Contours of constant growth rate σ_1 in the double long-wave limit. Instability to longitudinal vortex form in region I is dominated by real eigenmodes; in region II the instability is dominated by eigenmodes that are complex-conjugate pairs.

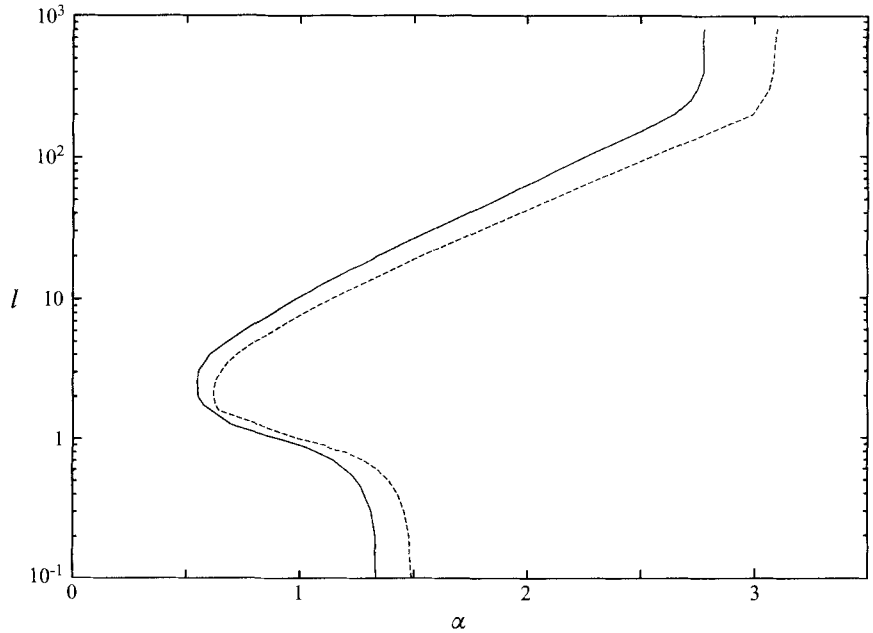

FIGURE 5. Locus of $l_{,\alpha}|_{\sigma_1} = 0$ in (α, l)-space: (see also figure 6); for power-law (solid line) and logarithmic (dashed line) mean velocity profiles.

$l \geqslant \sup\{\alpha\pi/6\gamma, \pi/\gamma\}$, we see that region II events can occur only with $\gamma \gg 1$, i.e. with rolls of large aspect ratio.

Figure 4 further suggests that the growth rate increases monotonically with increasing l (see also figure 6) and that (in region I) there is the minimum l, minimum α combination at which a particular growth rate can occur. The locus of points at which $l_{,\alpha}|_{\sigma_1} = 0$ thus represents the optimal α, l growth rate combination. So we turn

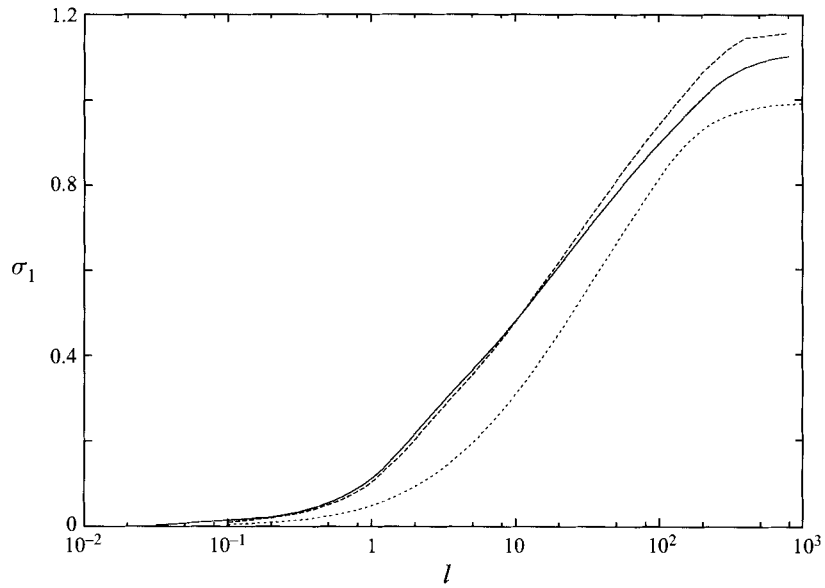

FIGURE 6. Curve of the growth rate σ_1 against spanwise wavenumber l along the locus at which $l_{,\alpha}|_{\sigma_1} = 0$ sketched in figure 5; power-law profile (solid line), logarithmic law (long dashes); growth rate for $\alpha = 6$ which is applicable (see text §5) to the data of Gong *et al.* 1996 (short dashes; see §5).

now to the full domain of $\sigma_1(\alpha, l)$ and plot this locus in (α, l)-space in figure 5; observe that it occurs when α is $O(1)$ for all l. We plot the growth rate along this locus in figure 6.

Finally we depict the eigenfunctions $\hat{\phi}$ and $\hat{u}$ in figures 7 and 8 respectively. Observe that for $l \gg 1$ distortion is confined to the lower portion of the domain and that it is then closely true that $\hat{\phi} \propto \hat{u}$.

4.4. *Logarithmic mean velocity profile*

Turbulent boundary layers have long been known to have mean velocity profiles that satisfy, in the overlapping portions of the wall and outer regions, the logarithmic law of the wall

$$\frac{\bar{u}U_\delta}{U_\tau} = \kappa^{-1}\ln\left(\frac{z\delta U_\tau}{\nu}\right) + C, \tag{4.5}$$

where U_τ is the wall velocity scale and κC is a constant whose value is determined by the level of roughness of the surface. So for completeness we should like to repeat our calculations with such a profile, assuming wavy terrain of equal amplitude to that in §§4.1–4.3 at $z = z_1$. Of course since the power-law and logarithmic law give rise to similar wave fields as we saw in figure 2, we should not expect greatly different results; and that is the case as we see by viewing figures 3, 5, 6, 7 and 8. We shall not comment further, but will outline how such calculations were made.

First, in accord with the non-dimensional scheme where U_δ is the reference velocity at $z = \delta$ and thus $\bar{u}(1) = 1$, we rewrite (4.5) as

$$\bar{u} = \ln(\mathrm{e}z^\beta) \quad \text{for} \quad z \in [z_1, 1 + z_1] \tag{4.6}$$

(where e is the exponential number). To arrive at this form we require $\mathrm{e}^{\kappa C\beta - 1}(\delta U_\tau/\nu)^\beta = 1$, where $\beta = U_\tau/U_\delta\kappa$ and, in order to exclude the critical layer at $\mathrm{e}z^\beta = 1$, demand

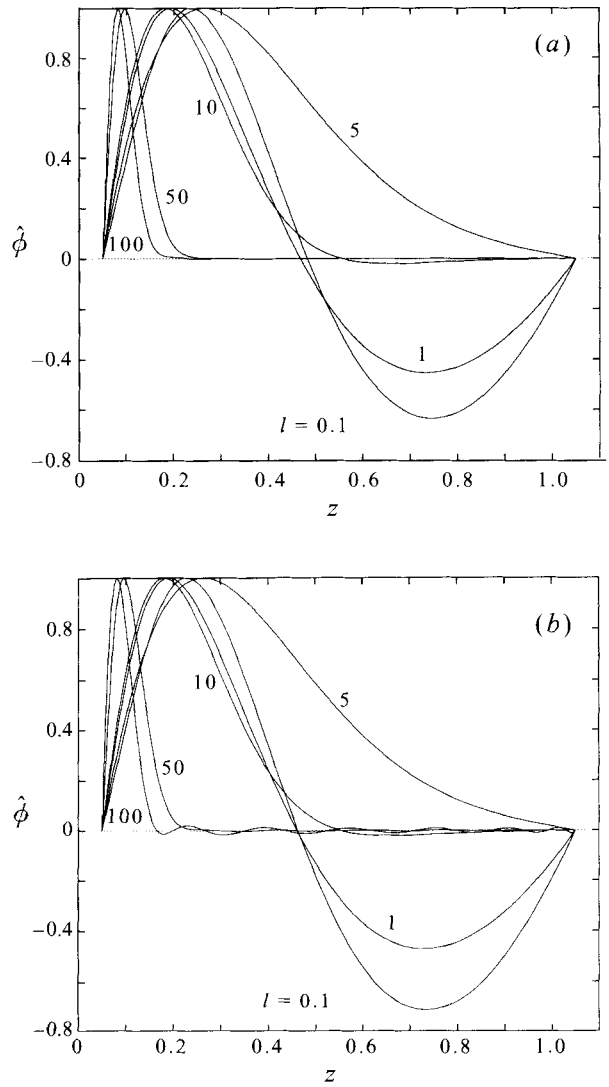

FIGURE 7. Eigenfunction $\hat{\phi}$ for $l = 0.1, 1, 5, 10, 50, 100$ and $\alpha = 1$; (*a*) power-law velocity profile; (*b*) logarithmic-law profile.

$ez_1^\beta > 1$; the constant β is then chosen accordingly. In fact we determine β by setting $z_1^q = \ln ez_1^\beta$, i.e. by equating $\bar{u}(z_1)$ with its counterpart in the example of §§4.1–4.3.

Then to ensure the terrain has the same amplitude at $z = z_1$ as in the power-law case, we set $\alpha\phi_1 = (\alpha z_1)^{1/2} K_{q-1/2}(\alpha z_1)$. The boundary condition at $z = 1 + z_1$, however, is less clear and so we solve (3.2) over the semi-infinite domain with $\alpha\phi \to 0$ as $\alpha z \to \infty$, which is known to be the case for type-2 waves (see §3.1); we then use that portion of the solution relevant to the domain $[z_1, 1 + z_1]$.

5. Comparison with experiment

Gong *et al.* (1996) conducted a wind tunnel study of the turbulent boundary layer that is formed over 16 rigid sinusoidal waves of amplitude a, wavelength λ and

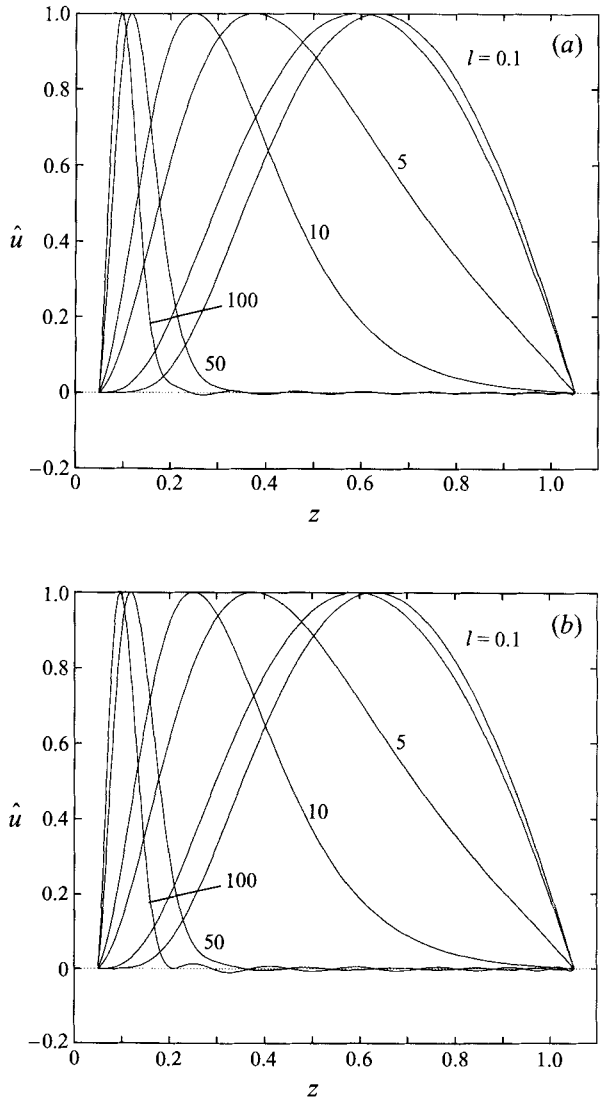

FIGURE 8. Eigenfunction $\hat{u}$ for $l = 0.1, 1, 5, 10, 50, 100$ and $\alpha = 1$; (*a*) power-law velocity profile; (*b*) logarithmic-law profile.

maximum wave slope $2\pi a/\lambda \approx 0.5$. The tunnel working section was about 3λ high, 4λ wide and 30λ long, where $\lambda \approx 0.61$ m. Two floor roughnesses, with roughness heights of 3×10^{-5} m and 40×10^{-5} m, were employed over the undulating portion of the floor and that preceding it. Both gave rise to a boundary layer that was turbulent well upstream of the first undulation, after which it grew to about λ thick, thereby suggesting $\alpha = 2\pi\delta/\lambda \approx 6$. The boundary layer was neutrally stratified and with zero pressure gradient with a free-stream velocity of about 10 m s^{-1}. Hot-wire anemometers were used to measure mean velocity and turbulence intensities and indicated, *inter alia*, that the flow was periodic by the fourth undulation. The data also indicated that a secondary flow, evident first in the initial trough, developed to saturation by the fourth wave crest, at which point it was seen to manifest as

circulations confined to the boundary layer with vorticity aligned with the flow; the cells had a vertical extent of approximately δ and three cell-pairs spanned the tunnel. This secondary flow was observed only above the smoother surface, however, to which the flow remained generally attached, not the rougher, where it separated. Further experiments by Miller (1995) (in another wind tunnel but using the same wavy wall) concur.

Our purpose here is to determine whether the instability giving rise to those longitudinal circulations is CL2-$O(1)$. There are of course other mechanisms that excite such circulations: the Taylor–Görtler and Benney-Lin (1960) instabilities for example, but each has features discordant with the experiment. First, Taylor–Görtler instability is associated with cells that are small with respect to the radius of curvature, a feature not present here, although it should be noted that CL2-$O(\epsilon^2)$ is akin, if only in an averaged sense, to Taylor–Görtler: i.e. CL2-$O(\epsilon^2)$ comes from an $O(\epsilon^2)$ *mean* curvature, not from an $O(\epsilon)$ *local* curvature that alters sign along the wave (Craik 1982*b*). It is also possible to have a local Taylor–Görtler instability that is distinct from CL2-$O(\epsilon^2)$. Second, Benney–Lin instability and its close relative CL1 (Craik & Leibovich 1976) presume an imposed wave field with spanwise structure, a feature also absent in the above experiment; and moreover, Benney–Lin and CL1 vortices grow algebraically rather than exponentially in time. Of course exponential growth need not be faster than linear growth if the early behaviour is relevant, but the rapidity with which the instability in the experiment saturates hints at exponential growth. Finally longitudinal vortices can also arise owing to nonlinear effects associated with unsteady (and viscous) critical layers (see e.g. Wu 1993), but here the critical layer is at the boundary, thereby excluding such instabilities.

There is therefore a *prima facie* case that the longitudinal vortices in the experiment are excited by the CL2-$O(1)$ instability, which as Phillips & Shen (1996) ascertained, and as we have seen in detail above, does operate in circumstances similar to those measured. Key features of CL2-$O(1)$ are an initially two-dimensional wave field described by neutral rotational Rayleigh waves (of slope characterized by the small parameter ϵ) interacting with $O(1)$ shear, exponential growth to longitudinal vortices, velocity perturbations in the y- and z-directions that are weaker by a factor of ϵ than their x-velocity perturbations and, at least for the cases so far considered in detail, $\hat{u}$ of one sign. Our intent then is to compare each of these features as calculated and as measured, beginning with the wave field.

Suppose then that beyond the fourth wave (where the flow is essentially periodic) the local mean velocity U can be decomposed as

$$U(X,Y,Z;\alpha) = \bar{U}(Z) + f(\alpha X)[\bar{U}_P(Z';\alpha X) + \tilde{U}(Z';\alpha X)\cos lY] + \check{U}(\alpha Z)\cos(\alpha X + \vartheta). \tag{5.1}$$

Here $\bar{U}$ and $\tilde{U}$ are experimental realizations of their lower-case counterparts, as are X, Y, Z, while $\check{U}$ is a streamwise-periodic velocity component due to the two-dimensional wave field; and, to ensure conservation of mass flux, we introduce the streamwise periodic factor $f(\alpha X) > 0$ such that $f(\alpha X + \pi/2) = f(\alpha X + 3\pi/2) = 1$. Concordant with the conservation of mass flux, the velocity components $\tilde{U}(Z';\alpha X)$ and $\bar{U}_P(Z';\alpha X)$ (later defined) are written in streamline variables Z', where $Z = Z' + h(X,Z')$, such that $h(X,0)$ specifies the terrain profile and $h(X,\infty) \to 0$, as is to be expected with type-2 waves. Finally, $\vartheta(\alpha Z)$ allows for any small phase shift with height as suggested by computations of turbulent shear flows over topography (Ayotte, Xu & Taylor 1994).

Then since U was measured on $Y = 0$ at $\alpha X_{11} + n\pi$, where $n = 0, \frac{1}{2}, 1, \frac{3}{2}, 2$ and

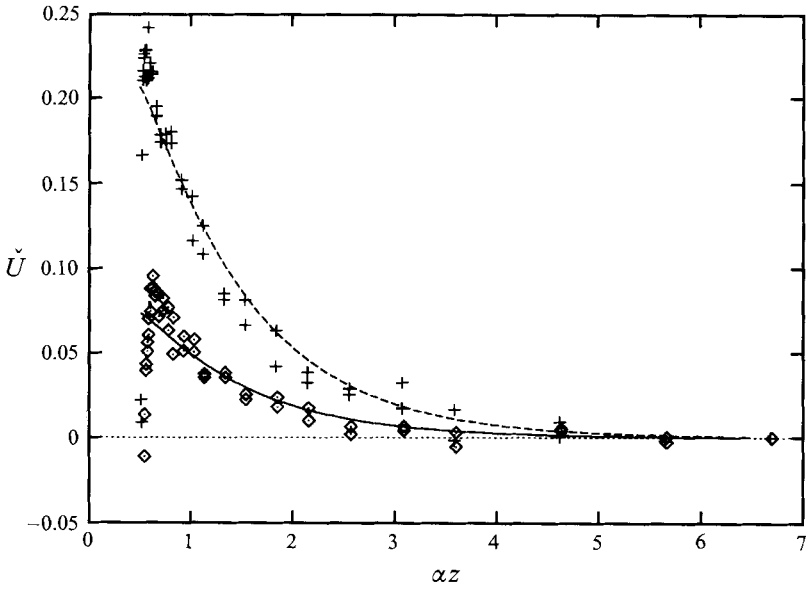

FIGURE 9. Plot of the amplitude of the streamwise periodic velocity perturbation caused by the undulating floor. Data of Gong *et al.* (1995) for flow over smooth (+) and rough (◇) undulations. Lines assume type-2 Rayleigh waves of similar peak amplitude.

αX_{11} is the crest of the eleventh undulation, we can deduce $\check{U}$ and $\bar{U} + \bar{U}_P + \tilde{U}$ for $Z \in (a/\delta, 1]$ as for example

$$\check{U} = \tfrac{1}{2}[U(\alpha X_{11}) - U(\alpha X_{11} + \pi)] + O(\epsilon^2) \tag{5.2}$$

and

$$\bar{U} + \bar{U}_P(\alpha X_{11} + \pi/2) + \tilde{U}(\alpha X_{11} + \pi/2) \approx \tfrac{1}{2}[U(\alpha X_{11}) + U(\alpha X_{11} + \pi)]. \tag{5.3}$$

We plot $\check{U}$ in figure 9. On the same plot are distributions of $\check{u} \propto \phi_{,z}$ (see §2) due to type-2 Rayleigh waves, where the constant of proportionality was chosen to match peak magnitudes. In both cases the decay in amplitude agrees very well with that of the data and there can be little question that the waves observed experimentally are indeed type-2 Rayleigh waves. Note that the amplitude of the fluctuating velocity field over the rougher undulations is significantly lower than that over the smoother ones, a consequence no doubt of the lee slope and trough separation occurring on the former. Moreover while (the variance of) streamwise turbulence fluctuations (not shown, see figure 7 of Gong *et al.*) exceed the amplitude of the wave-induced velocity field over the rougher wall, the converse is true (over some z at least) over the smoother wall.

Now finite-amplitude wave equilibria induce their own Reynolds stress field – sometimes referred to as a wave-supported stress or, in GLM terms, a Stokes drift component in the z-direction – which results in a mean velocity field different from the undisturbed one (Nöther 1921). We think of this velocity field anomaly as a primary instability and denote the ensuing spanwise-independent velocity component $\bar{U}_P$. The sum $\bar{U} + \bar{U}_P + \tilde{U}$ is plotted in figure 10, along with logarithmic distributions in z of slope β, which we assume approximate $\bar{U}$. Note that the slope β is known (as an average over the wavelength) in each case. Interestingly, an outer region, i.e. a velocity in excess of the logarithmic variation, is evident over the rougher waves but not the smoother ones, suggesting, in accord with our comment in the previous

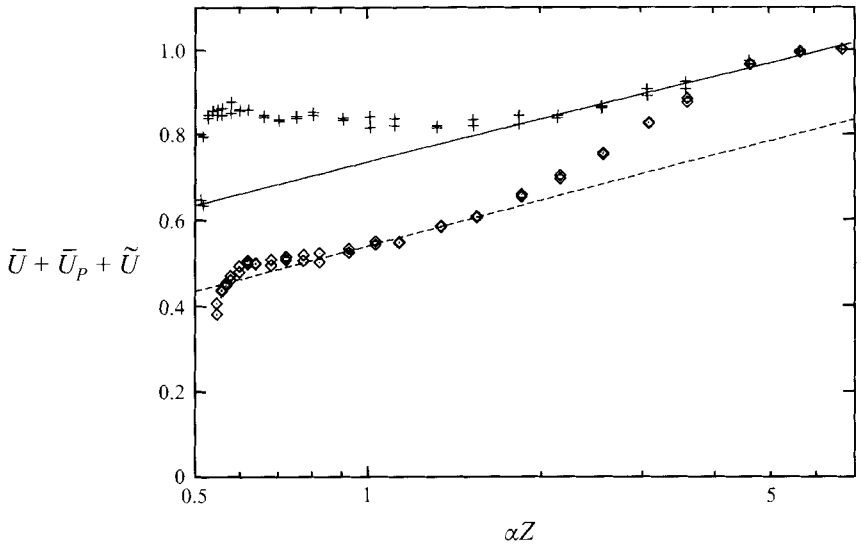

FIGURE 10. Plot of the sum of the mean velocity $\bar{U}$, the component resulting from the primary instability $\bar{U}_P$, and that due to the secondary instability $\tilde{U}$. Data of Gong *et al.* (1995) for flow over smooth + and rough ◇ undulations. Lines represent $\bar{U}$ with slope determined by the average shear stress over the wavelength.

paragraph, that while turbulence dominates the former flow, Rayleigh waves dominate the latter. Furthermore while the difference $\bar{U}_P+\tilde{U}$ near the wall is only slightly larger than experimental scatter for the rougher wave case, it peaks at about 0.2 for the smoother.

The wave slope is a maximum at the wall and diminishes rapidly and monotonically with height (see (4.2)). In the experiment that maximum is about 0.5 and if we denote that wave slope ϵ_E, then $2\pi a/10\lambda < O(\epsilon_E) < 2\pi a/\lambda$. The analysis however is based on the premise that ϵ is less than $O(1)$, to wit $1/10\sqrt{10} < O(\epsilon) < 1/\sqrt{10}$, so that although ϵ_E falls within the bounds of the analysis for much of the boundary layer, there is a region close to the wall where is does not. We must therefore ask what influence the wave slope has on the instability mechanism and ascertain at what slope effects not currently included in the analysis become important. Full details will be given elsewhere, but it transpires that CL2-$O(1)$ remains the underlying instability mechanism for waves of $O(\epsilon_E)$, although other influences, in particular the wave-supported stress, play a small role. Unfortunately whether that role acts to enhance or diminish the growth rate is not yet clear.

The velocity perturbation $\tilde{U}$ due to the secondary flow is plotted in figure 11. $\tilde{U}$ varies spanwise and velocity traverses suggest that $\alpha/l \approx \frac{4}{3}$, so plotted also and scaled to peak in accord with the data is the profile for $\tilde{u}$ at $\alpha = 6$, $l = 3\alpha/4$. Of course $\tilde{u}$ is an eigenfunction relevant to the initial stages of the instability, while $\tilde{U}$ is pursuant to an equilibrated state in which nonlinearities have no doubt come into play. Nevertheless $\tilde{u}$ and $\tilde{U}$ are of the same sign and have similar characteristics. As an aside we note that theorists have long conjectured that provided the eigenfunction is set before nonlinearities come into play then its functional form remains essentially unchanged in the nonlinear regime. Formal justification for this conjecture is wanting, but as we can see it is well supported in the present context. In view of this we use our knowledge of $\bar{U}_P+\tilde{U}$ and $\tilde{u}$ to estimate $\bar{U}_P$, which is also plotted in figure 11.

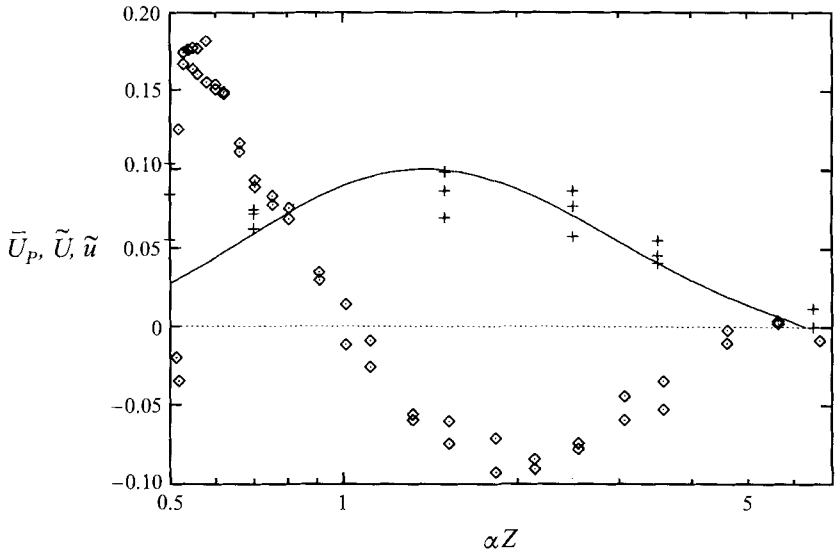

FIGURE 11. Plot of the of the mean velocity component resulting from the primary instability $\bar{U}_P$ ($\diamond$), and that due to the secondary instability $\tilde{U}$ (+) each evaluated midway between the crest and trough. Data of Gong *et al.* (1995) for flow over smooth undulations. Solid line depicts $\tilde{u}$ for $\alpha = 6$ and $l = 0.75\alpha$ scaled to peak at 0.1.

Note that the sign of $\bar{U}_P$ changes with z; this feature is also observed in atmospheric boundary layers over ocean waves (Miller *et al.* 1995).

We turn now to the growth rate of the secondary flow and note that spanwise variations in mean velocity were first evident in the trough of the first undulation; moreover they were seen to persist and rapidly grow over the first few undulations, at which point they saturate. Our object is to determine whether such growth is exponential. Consider first the ratio of transverse to streamwise velocity components. In §2 we found that $\tilde{w}/\tilde{u} = O(\epsilon)$ for CL2-$O(1)$ while from experiment $\tilde{W}_{\max}/\tilde{U}_{\max} \approx \frac{1}{2}$ which, since $2\pi a/10\lambda < O(\epsilon_E) < 2\pi a/\lambda$, concurs, just. In consequence we may use (2.5) and (4.6) to estimate the growth rate as $\sigma_1 = -\hat{w}\beta/\hat{u}z \equiv -\tilde{W}\beta/\tilde{U}Z$. Now figure 11 suggests that $\tilde{U}$ has its peak at some $Z \in (0.1, 0.4)$ and since $\beta \approx 0.145$ for the smoother undulations, we find (in accord with figure 6) that, $\sigma_1 \in (0.2, 0.7)$. Finally since it takes about 0.4 s for the flow to traverse the first four peaks, $t = 0.4U_\delta/\delta \approx 6.7$ and thus $\sigma t = \epsilon_E \sigma_1 t \in (0.6, 2.3)$; but does σt act exponentially?

In order to answer this question consider the exponential growth scenario suggested by (2.2), namely $[\tilde{U}_{max}, \tilde{W}_{max}] = \Delta[e^{\sigma t}, \epsilon_E e^{\sigma t}]$. Now $\tilde{W}_{max} \approx \pm 0.05$ and $\tilde{U}_{max} \approx \pm 0.1$ by the fourth crest, so to realize $\tilde{W}_{max}$ our initial perturbation Δ must lie between ± 0.01 and ± 0.05. Since the upper bound exceeds the ± 0.02 scatter in velocity measurements at the crest of the first undulation it must be excluded, but the lower bound is admissible; furthermore it leads to $\tilde{U}_{max} \approx \pm 0.1$ as it should. In short, the experimental results are consistent with exponential growth. Algebraic growth on the other hand can require hundreds of wave periods to induce well-developed circulations, as Faller (1978) and Faller & Caponi (1978) discovered in experiments designed to reproduce the CL1 instability.

Thus since the undulations in Gong *et al.*'s experiment do excite type-2 Rayleigh waves, and since the interaction of those waves with the mean shear does excite a secondary flow in which transverse velocity components are ϵ_E smaller than axial;

and since the secondary flow, which manifests as longitudinal vortices, initially grows exponentially fast we conclude that Gong *et al.* do observe circulations arising via the CL2-$O(1)$ instability. But having come to that conclusion we must ask why CL2-$O(1)$ is observed only above the smoother undulations? We give two possible explanations, both related to the amplitude of $\breve{U}$ which is considerably lower over the rougher waves. The first is that circulations do indeed form, but that they are not observed because they are weaker and fall within the range of noise associated with data measurement. And/or second, because the streamwise turbulence fluctuations are of comparable or larger amplitude than $\breve{U}$ over the rougher waves, turbulence dominates the flow field thereby hampering and possibly obliterating the relatively large circulations.

6. Discussion

Our study indicates that parallel inviscid $O(1)$ shear with a representative velocity distribution interacting with $O(\epsilon)$ spanwise-independent type-2 Rayleigh waves, is an appropriate model for non-separating turbulent boundary layer flow over small-amplitude rigid wavy terrain. Both the model and experiment depict an instability to longitudinal vortex form. Analysis indicates that the instability is CL2-$O(1)$ and because the experiments concur with crucial aspects of our calculations, we conclude that the longitudinal vortices excited therein are also excited by CL2-$O(1)$. This represents the first time that CL2-$O(1)$ has been identified in a physical situation.

But the calculations are wanting in some respects: first, finite-amplitude waves induce their own Reynolds stress and thus velocity field anomaly. This field is identifiable in the experiment but is ignored in the analysis. Serendipitously, vastly different mean velocity profiles do not appear to greatly affect $\tilde{u}(z;\alpha,l)$ – compare our eigenfunctions with those of Phillips & Wu (1994) for example – although just how, if at all, an $O(\epsilon^2)$ (spanwise independent) correction to the mean velocity profile due to a primary instability affects the growth rate of the secondary instability, is unclear.

Second, we ignore interaction with the turbulence field. This would appear to be justified if velocity fluctuations associated with the waves well exceed, over at least part of the domain, the streamwise turbulence intensity. If the converse is true the turbulence motions apparently swamp or at least dramatically curtail the growth of longitudinal vortices. In short the occurrence or dominance of CL2-$O(1)$ is affected by the relative amplitudes of the wave and turbulence fluctuations.

Third, our calculations indicate that the growth rate of the secondary flow increases with l and is most unstable in the short-wave limit $l^2 \to \infty$. Nature, however, chooses a slower growth rate, specifically that for which l is close to the lower bound peculiar to boundary layer flow over wavy terrain, given by $l = \sup\{\alpha\pi/6\gamma, \pi/\gamma\}$ – although whether smaller faster growing cell pairs also form but are not observed or are overwhelmed by nonlinearities or their larger confreres, is unclear. Similar disparities were observed by Poje & Lumley (1995) in their studies of coherent motions in the wall region of turbulent boundary layers. Following Lumley (1971) they note that although modes given by higher spanwise wavenumbers are better able to extract energy from a fixed spatial mean, they lose energy faster to the background turbulence. Accordingly while lower wavenumber modes are less affected by nonlinear interactions with the mean, they grow so slowly that constant energy loss to the background turbulence over time limits their maximum amplitude. In consequence the coherent or secondary mean velocity field is that mode that most effectively extracts energy in a volume-averaged sense from the mean motion, while minimizing energy loss to both viscous

dissipation and small-scale turbulence. Of course the coherent structures that Poje & Lumley have in mind have a vertical extent of perhaps 50 wall units, whereas those under consideration extend, since $\gamma = 4\pi/3\alpha \approx 2/3$, to the limits of the boundary layer. Nevertheless it appears that much the same type of optimization process may obtain in each.

We should like to thank Wanmin Gong and Peter Taylor for use of their data prior to its publication and Julian Hunt for bringing it to our attention. The work was supported by National Science Foundation grants CTS-9008477 and OCE-9503456.

REFERENCES

ABRAMOWITZ, M. & STEGUN, I. A. 1965 *Handbook of Mathematical Functions*. Dover.

ALPERS, W. & BRÜMMER, B. 1994 Atmospheric boundary layer rolls observed by the synthetic aperture radar aboard the ERS-1 satellite. *J. Geophys. Res.* **99**, 12613–12621.

ANDREWS, D. G. & MCINTYRE, M. E. 1978 An exact theory of nonlinear waves on a Lagrangian-mean flow. *J. Fluid Mech.* **89**, 609–646.

AYOTTE, K. W., XU, D. & TAYLOR, P. A. 1994 The impact of different turbulent closures on predictions of the mixed spectral finite difference model for flow over topography. *Boundary-Layer Met.* **68**, 1–33.

BENNEY, D. J. & LIN, C. C. 1960 On the secondary motion induced by oscillations in a shear flow. *Phys. Fluids* **3**, 656–657.

CRAIK, A. D. D. 1977 The generation of Langmuir circulations by an instability mechanism. *J. Fluid Mech.* **81**, 209–223.

CRAIK, A. D. D. 1982*a* The generalized Lagrangian-mean equations and hydrodynamic stability. *J. Fluid Mech.* **125**, 27–35.

CRAIK, A. D. D. 1982*b* Wave-induced longitudinal-vortex instability in shear layers. *J. Fluid Mech.* **125**, 37–52.

CRAIK, A. D. D. 1985 *Wave Interactions and Fluid Flows*. Cambridge University Press.

CRAIK, A. D. D. & LEIBOVICH, S. 1976 A rational model for Langmuir circulations. *J. Fluid Mech.* **73** 401–426.

FALLER, A. J. 1978 Experiments with controlled Langmuir circulations. *Science* **201**, 618–620.

FALLER, A. J. & CAPONI, E. A. 1978 Laboratory studies of wind-driven Langmuir circulations. *J. Geophys. Res.* **83**, 3617–3633.

GONG, W., TAYLOR, P. A. & DÖRNBRACK, A. 1996 Turbulent boundary-layer flow over fixed, aerodynamically rough two-dimensional sinusoidal waves. *J. Fluid Mech.* **312**, 1–37.

HUNT, J. C. R., LALAS, D. P. & ASIMAKOPOULOS, D. N. 1984 Air flow and dispersion in rough terrain: a report on Euromech 173. *J. Fluid Mech.* **142**, 201–216.

HUNT, J. C. R., TAMPIERI, F., WENG, W. S. & CARRUTHERS, D. J. 1991 Air flow and dispersion in rough terrain: a colloquium and a computational workshop. *J. Fluid Mech.* **227**, 667–688.

LANGMUIR, I. 1938 Surface motion of water induced by wind. *Science* **87**, 119–123.

LEIBOVICH, S. 1977 Convective instability of stably stratified water in the ocean. *J. Fluid Mech.* **82**, 561–585.

LEIBOVICH, S. 1983 The form and dynamics of Langmiur circulations. *Ann. Rev. Fluid Mech.* **15**, 391–427.

LEMONE, M. 1973 The structure and dynamics of horizontal roll vortices in the planetary boundary layer. *J. Atmos. Sci.* **30**, 1077–1091.

LUMLEY, J. L. 1971 Some comments on the energy method. In *Developments in Mechanics 6* (ed. L. Lee & A. Szewczyk). Notre Dame Press.

MILLER, C. A. 1995 Turbulent boundary layers above complex terrain. PhD thesis, University of Western Ontario.

MILLER, S., FRIEHE, C., HRISTOV, T. & EDSON, J. 1995 Wind profile and turbulence over ocean waves. *Bull. Am. Phys. Soc.* **40**, 1971.

NÖTHER, F. 1921 Das Turbulenaproblem *Z. Angew. Math. Mech.* **1**, 125.

PHILLIPS, W. R. C. & SHEN, Q. 1996 On a family of wave-mean shear interactions and their instability to longitudinal vortex form. *Stud. Appl. Maths* **96**, 143–161.

PHILLIPS, W. R. C. & WU, Z. 1994 On the instability of wave-catalysed longitudinal vortices in strong shear. *J. Fluid Mech.* **272**, 235–254.

POJE, A. C. & LUMLEY, J. L. 1995 A model for large-scale structures in turbulent shear flows. *J. Fluid Mech.* **285**, 349–369.

STULL, R. B. 1988 *An Introduction to Boundary-Layer Meteorology*. Kluwer.

WU, X. 1993 Nonlinear temporal-spatial modulation of near planar Rayleigh waves in shear flows: formation of streamwise vortices. *J. Fluid Mech.* **256**, 685–719.